Eur. Phys. J. B **21**, 163–174 (2001)

THE EUROPEAN PHYSICAL JOURNAL B

EDP Sciences

Interplay of structural, magnetic and transport properties in the layered Co-based perovskite $LnBaCo_2O_5$ (Ln = Tb, Dy, Ho)

F. Fauth[1,a], E. Suard[2], V. Caignaert[3], B. Domengès[3], I. Mirebeau[4], and L. Keller[5]

[1] Swiss Light Source, Paul Scherrer Institut, 5232 Villigen PSI, Switzerland
[2] Institut Laue Langevin, 6, rue Jules Horowitz, BP 156X, 38042 Grenoble Cedex 9, France
[3] Laboratoire CRISMAT/ISMRA, boulevard du Maréchal Juin, 14050 Caen Cedex, France
[4] Laboratoire Léon Brillouin, CE-Saclay, 91191 Gif-sur-Yvette, France
[5] Laboratory for Neutron Scattering, Paul Scherrer Institut, 5232 Villigen PSI, Switzerland

Received 13 December 2000

Abstract. The oxygen deficient cobaltites $LnBaCo_2O_5$ (Ln = Tb, Dy, Ho) exhibit two successive crystallographic transitions at T_N ∼340 K and at T_{CO} ∼210 K. Whereas the first transition (P4/mmm to Pmmm) is related to the long-range antiferromagnetic ordering of the Co ions (spin ordering), the second transition (Pmmm to Pmmb) corresponds to the long-range ordering of the Co^{2+} and Co^{3+} species (charge ordering) occurring in 1:1 ratio in the structure. The charge ordered (CO) state was directly evidenced by the observation of additional superstructure peaks using neutron and electron diffraction techniques. The CO state was also confirmed indirectly from refinement of high resolution neutron diffraction data as well as from resistivity and DSC measurements. From the refined saturated magnetic moment values only, $\sim 3.7\mu_B$ and $\sim 2.7\mu_B$, the electronic configuration of the Co ions in $LnBaCo_2O_5$ remains conjectural. Two pictures, with Co^{3+} ions either in intermediate spin state ($t_{2g}^5 e_g^1$) or in high spin state ($t_{2g}^4 e_g^2$), describe equally well our experimental data. In both cases, the observed magnetic structure can be explained using the qualitative Goodenough-Kanamori rules for superexchange. Finally, in contrast to the parent Ln = Y compound [Vogt *et al.*, Phys. Rev. Lett. **84**, 2969 (2000)], we do not report any spin transition in $LnBaCo_2O_5$ (Ln = Tb, Dy, Ho).

PACS. 61.12.-q Neutron diffraction and scattering – 71.30.+h Metal-insulator transitions and other electronic transitions – 75.50.Ee Antiferromagnetics

1 Introduction

The perovskite oxides ABO_3 (A is either a trivalent lanthanide, a divalent alkaline or a mixing of both and B a transition metal) and their derived compounds, have always attracted much interest since they display strong correlation between their crystallographic, magnetic and transport properties. This is mainly due to the strong overlap of the unfilled, and therefore magnetic, $3d$ electron orbitals of the transition metal element with the oxygen $2p$ and/or $1s$ orbitals. During the last few years, there was a large number of research activities on the Mn oxides of general type $A_{1-x}A'_xMnO_3$ in order to explain the mechanism leading to the colossal-magnetoresistivy (CMR) observed in these materials. In the cobaltites $La_{1-x}Sr_xCoO_3$ [1], MR properties were also reported, but with a much smaller magnitude than in the manganites. Up to now, the highest MR ratios ever observed in Co-based oxides were found in the layered perovskite-based compounds $LnBaCo_2O_{5.4}$ (Ln = Eu, Gd) [2]. These systems, of general description $LnBaCo_2O_{5+\delta}$ (Ln = Lanthanide and $0 \leq \delta \leq 1$), are particularly interesting since they also display a large variety of magnetic and transport properties, which themselves depend on the tunable oxygen concentration [3–7]. Similarly to what was observed in the manganites, it is likely that the magnetic and transport behavior in $LnBaCo_2O_{5+\delta}$ is driven by the mixed valence state of the cobalt ions, which is expressed by the relations Co^{2+}:Co^{3+} = $(\frac{1}{2} - \delta)$:$(\frac{1}{2} + \delta)$ for $0.5 \leq \delta$ and Co^{4+}:Co^{3+} = $(\delta - \frac{1}{2})$:$(\frac{3}{2} - \delta)$ for $\delta \leq 0.5$.

Of course, the wide allowed oxygen range in $LnBaCo_2O_{5+\delta}$ ($0 \leq \delta \leq 1$) also leads to several crystallographic structures, with either pyramidal or octahedral environments (or both) for the Co ions [3,5,8–12]. The crystal structure of $LnBaCo_2O_{5+\delta}$ corresponds roughly to the doubling of the original perovskite cell (so called '$a_p \times a_p \times 2a_p$'-phase, where a_p refers to the cubic perovskite cell parameter). This doubling accounts of the alternating BaO and LnO_δ layers along one crystallographic

[a] *Present address*: European Synchrotron Radiation Facility, BP 220, 38043 Grenoble Cedex, France
e-mail: `fauth@esrf.fr`

axis. This layered structure is as best observed in the oxygen deficient case, $LnBaCo_2O_5$, since it is assumed the oxygen ions are absent of one of the Ln or Ba layer. Thus, the Co^{3+} and Co^{2+} ions are within square base pyramids formed by the five oxygen neighbors. In the stoichiometric case, $LnBaCo_2O_6$, all the Co^{4+} and Co^{3+} ions are octahedrally coordinated. Here, the layered structure is not as evident as in the $\delta = 0$ case since it would only result from an ordering of the Ln and Ba ions. In $LaBaCo_2O_6$, the only $LnBaCo_2O_6$ compound which has been studied by neutron powder diffraction so far, the crystal structure at room temperature is the pure cubic perovskite one, meaning the Ln and Ba ions are statistically distributed on the same site [11]. However, this can be due in this particular case to the similar size of the La and Ba ions. Thus, a layered structure is likely to occur in $LnBaCo_2O_6$ with smaller lanthanide. In the intermediate cases, $LnBaCo_2O_{5+\delta}$ ($\delta \neq 0, 1$), the exact crystal structure is still not clearly established. Worse rather confusing results have been reported up to now, more particularly for the $\delta = 0.5$ case [4–8,12–14]. In $LnBaCo_2O_{5.5}$, a '$a_p \times 2a_p \times 2a_p$'-type structure is generally assumed, with Co^{3+} ions equally distributed in pyramidal and octahedral oxygen environment [12,14]. The change from pyramidal to octahedral oxygen environment is not without consequences on the electronic configuration of the Co ions since it significantly affects the crystalline electric field acting on the cobalt site [15].

Since there are only few examples of Co ions in pyramidal environment ($Sr_2Y_{0.8}Ca_{0.2}Co_2O_6$ [16], $Ln_2BaCo_2O_5$ (Ln = Y, Ho-Lu) [17], $Sr_4Fe_4Co_2O_{13}$ [18]), the electronic state of Co ions in pyramids remains a relatively unknown subject compared to the problematic of 3*d* transitions elements in octahedral and/or tetrahedral environment. When further considering that Co^{2+}, Co^{3+} and Co^{4+} ions are all susceptible to exist in multiple spin states, it is likely that the $LnBaCo_2O_{5+\delta}$ systems have the potential to reproduce most of the possible electronic configurations of the Co ion. For this reason already, these layered cobaltite compounds deserve an intensive study. Very recently, neutron and synchrotron powder diffraction results have been published for $YBaCo_2O_5$ [9] and $HoBaCo_2O_5$ [10], with however contradictory conclusions on the actual electronic state of the Co ions. More surprisingly, exactly the same discrepancy occurs in two successive band structure calculation studies performed on the basis of the $YBaCo_2O_5$ structural data [19,20]. Hence, similarly to the famous $La_{1-x}Sr_xCoO_3$ system, the exact electronic configuration of cobalt ions in $LnBaCo_2O_{5+\delta}$ already represents a challenge. Furthermore, the difficulty in determining the electronic state of Co ions in oxides is also enhanced by the non negligible orbital contribution to the magnetic moment. Beside an hypothetical spin state transition, the $LnBaCo_2O_{5+\delta}$ system is also a good candidate for the onset of charge ordering. In $A_{1-x}A'_xMnO_3$ type CMR compounds, charge ordering of the Mn^{3+} and Mn^{4+} ions were best observed for $x = 0.5$, that is for a 1:1 ratio of both Mn species. Therefore, charge ordering is most likely to occur in the particular $LnBaCo_2O_5$ and $LnBaCo_2O_6$ compounds for which Co^{2+}:Co^{3+} and Co^{3+}:Co^{4+} ions are in 1:1 ratio, respectively. In this paper we focus on the oxygen deficient compounds $LnBaCo_2O_{5.00}$ (Ln = Tb, Dy, Ho) which exhibit orbital and charge ordering at temperatures far below the onset of antiferromagnetic ordering. We carefully describe several experimental procedures enabling to evidence and characterize the onset of the long-range charge ordered phase. Finally, we discuss within the framework of Goodenough-Kanamori (GK) rules for superexchange magnetism [21,22] both the equally probable models for the electronic configuration of the Co^{2+} and Co^{3+} species occurring in $LnBaCo_2O_5$.

2 Experimental

The $LnBaCo_2O_5$ samples (Ln = Tb, Dy, Ho) were synthesized using a two step method which was already successfully applied to produce the compound $YBaMn_2O_5$ [23]. The oxides Ln_2O_3, Co_3O_4 and $BaCO_3$ were mixed in the appropriate ratio, then ground and sintered several times, first up to 1000 °C in order to achieve complete decarbonation, and finally to 1150 °C. The samples were cooled down to room temperature under air atmosphere, resulting in a significant oxygen excess for the as-synthesized samples $LnBaCo_2O_{5+\delta_o}$ ($\delta_o \neq 0$). Note that δ_o appears to depend on the Ln cation [5]. In order to achieve the pure deficient compounds, the samples were heated up again and cooled down under an Ar-flow reduced atmosphere. The oxygen stoichiometry of our $LnBaCo_2O_{5+\delta}$ compounds was definitively determined from the neutron powder diffraction (NPD) experiments. High resolution NPD experiments were performed on the diffractometers D1A ($\lambda = 1.911$ Å) and D2B ($\lambda = 1.594$ Å) at the institute Laue-Langevin (ILL) in Grenoble. The samples were measured at several temperatures ranging from 1.5 K to 375 K. An improved accuracy in the magnitude of the individual temperature factors was obtained by collecting additional patterns on D2B using a shorter wavelength ($\lambda = 1.05$ Å). Due to the weakness of the superstructure peaks induced by the charge ordering, further measurements were performed for Ln = Tb, Ho on the G6-1 diffractometer at the Laboratoire Léon Brillouin in Saclay. There, the combined use of cold neutrons ($\lambda = 4.75$ Å), of a pyrolitic graphite monochromator and of a 400-cells position sensitive detector, provided powder patterns with remarkably high signal to background ratio. This condition was necessary in order to correctly determine the charge ordered phase of $LnBaCo_2O_5$ and follow the intensity of the superstructure peaks. To better characterize the rare earth magnetism in $TbBaCo_2O_5$, additional data were collected in temperature range 1.5–15 K using the D1B ($\lambda = 2.52$ Å) diffractometer of the ILL. Finally, some of the $DyBaCo_2O_5$ data were collected using the DMC diffractometer ($\lambda = 2.568$ Å and $\lambda = 4.208$ Å) at the SINQ facility of the Paul Sherrer Institute (Villigen). All the NPD data were refined by the Rietveld method using the program FULLPROF [24]. Absorption corrections were appropriately taken into consideration. In all three compounds, the linear absorption coefficient was measured on

D1A at $\lambda = 1.911$ Å and linearly extrapolated for the other wavelengths. In the case of Ln = Dy, the absorption effects were minimized by using a double cylinder container. At the same temperature, NPD data collected with different instruments and/or at different wavelengths on D2B were refined simultaneously. Output from FULLPROF were then used for Bond Valence Calculations using the software package *VaList* [25]. In order to confirm the crystallographic origin of the superstructure peaks previously measured on G6-1, electron diffraction experiments were performed on a JEM2010 operating at 200 kV and equipped with a ±30° double tilt cooling holder allowing observations from low temperature (93 K) to room temperature. For additional microdiffraction experiments, we used a 20 micron diameter condenser aperture and a 25 nm nanoprobe. Differential scanning calorimetry (DSC) measurements were performed on $LnBaCo_2O_5$ using either a Seiko DSC220C (Ln = Ho,Tb) or a TA-Instruments DSC2920 (Ln = Dy) microcalorimeter. Resistivity measurements were performed using the standard four points technique on $HoBaCo_2O_5$ and $TbBaCo_2O_5$ over a significant temperature range, with and without application of an external magnetic field of 5 tesla. AC-resistivity data were registered on both heating and cooling modes (1°/min) with however no significant differences in the results.

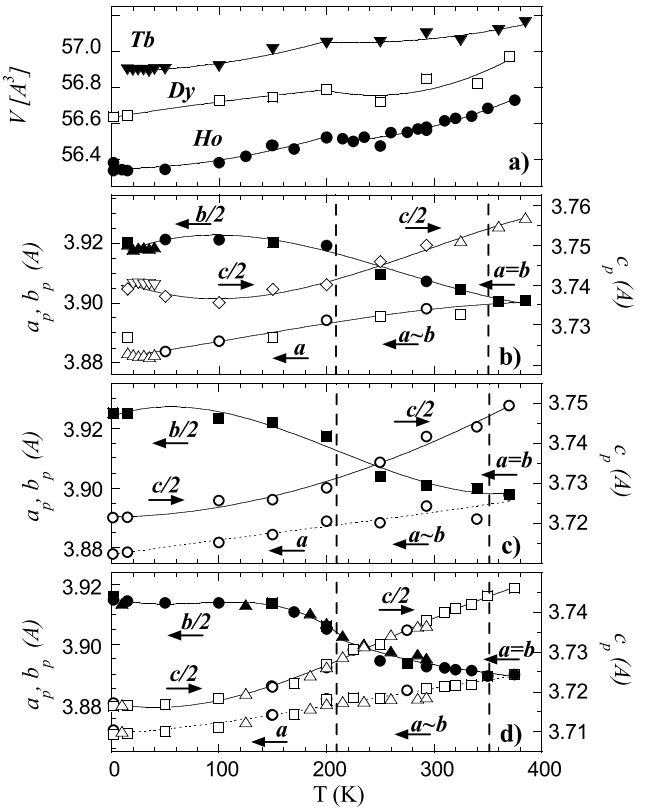

Fig. 1. Temperature dependence of the (a) volume and pseudocubic cell parameters in (b) $TbBaCo_2O_5$, (c) $DyBaCo_2O_5$ and (d) $HoBaCo_2O_5$. The lines are guide to the eye and the different symbols refer to data collected on different instruments.

3 Structural aspects

3.1 Charge disordered phase

At high temperature (340 K $\lesssim T$), all $LnBaCo_2O_5$ (Ln = Tb, Dy, Ho) samples are paramagnetic and the crystallographic structure is tetragonal. NPD patterns were refined using the P4/mmm space group with cell parameters $a = a_p$ and $c \sim 2a_p$. Here a_p refers to the cell parameter of the cubic perovskite lattice. In $TbBaCo_2O_5$, we noticed an extra impurity peak attributed to the presence of a very small amount of CoO in the phase (less than 1% in mass as obtained from quantitative Rietveld refinement). The identification of CoO as the impurity phase was confirmed by the onset of an additional magnetic peak below room temperature in accordance to the antiferromagnetic structure of CoO. Consequently, the crystal and magnetic (when appropriate) structure of CoO was included in the refinements of all $TbBaCo_2O_5$ patterns. The crystal structure of $LnBaCo_2O_5$ (Ln = Tb, Dy, Ho) in the paramagnetic phase corresponds exactly to the assumed layered structure with oxygen atoms fully occupying the Ba layers and the Ln layers free of oxygen (see Tab. 1). Cobalt atoms are in corner shared square base pyramids formed by the oxygen neighbors, whereas the Ln and Ba atoms are ordered and form alternated layers along the *c*-direction. Bond Valence calculations gave satisfactory results for all cations and provided the Co site are occupied by cations in the mixed valence state ∼2.4. This fairly corresponds to the expected value for a statistical occupation of Co^{2+} and Co^{3+} in a 1:1 ratio. At this point of the refinement, the oxygen stoichiometry of all compounds was checked by adding extra oxygen ions in the Ln layer and refining the occupancy. In all cases, the occupation factor of this additional site remains zero within the error bars (±0.01), thus proving the formula is really $LnBaCo_2O_{5+00}$ for all three Ln = Tb, Dy and Ho samples.

When lowering the temperature below $T_N \sim 340$ K, $LnBaCo_2O_5$ (Ln = Tb, Dy, Ho) undergo a magnetic transition to an antiferromagnetic structure which itself induces an orthorhombic distortion of the unit-cell. The new crystallographic space group is Pmmm with cell parameters $a \sim b \sim a_p$ and $c \sim 2a_p$, $((b-a)/(b+a) \sim 5 \times 10^{-4})$. Consequently, the basis of the CoO_5 pyramids is now formed by two different Co-O distances. Furthermore, the oxygen atoms O1 and O2 forming the basal plane of the pyramids are free to move independently along the *c*-direction. In this structure, the Co site is still occupied by Co cations in a mixed valence state. As shown in Figures 1 and 2, the cell volume and the Co-O distances of the Pmmm phase do not exhibit any discontinuity at T_N. Otherwise, the new orthorhombic structure remains globally the same as the high temperature paramagnetic phase (Tab. 1).

Table 1. Refined structural parameters, selected bond lengths and magnetic moments in the charge disordered state of $LnBaCo_2O_5$. Atomic positions in the paramagnetic phase (P4/mmm) are ($\frac{1}{2}$,$\frac{1}{2}$,0) for Ln; ($\frac{1}{2}$,$\frac{1}{2}$,$\frac{1}{2}$) for Ba; (0,0,z) for Co and (0,$\frac{1}{2}$,z) for O(1). In the antiferromagnetic phase (Pmmm) the oxygen site is splitted into two sites: (0,$\frac{1}{2}$,z) for O(1), ($\frac{1}{2}$,0,z) for O(2) and (0,0,$\frac{1}{2}$) for O(4). In P4/mmm, O(1) and O(2) sites are equivalent.

	$TbBaCo_2O_5$		$DyBaCo_2O_5$	$HoBaCo_2O_5$	
	385 K	250 K	375 K	275 K	293 K
S.G.	P4/mmm	Pmmm	Pmmm	P4/mmm	Pmmm
a Å	3.9007(1)	3.8971(1)	3.8937(1)	3.8915(1)	3.8871(1)
b Å	-	3.9088(1)	3.8998(1)	-	3.8946(1)
c Å	7.5137(1)	7.4906(2)	7.4815(1)	7.4921(2)	7.4709(1)
z_{Co}	0.2433(4)	0.2433(5)	0.2424(4)	0.2409(6)	0.2407(4)
$z_{O(1)}$	0.1923(1)	0.1908(7)	0.1932(5)	0.1884(2)	0.1912(5)
$z_{O(2)}$	-	0.1935(7)	0.1862(5)	-	0.1862(5)
Co-O(1) Å	4×1.988(1)	2×1.994(3)	2×1.984(2)	4×1.985(2)	2×1.982(2)
Co-O(2) Å	-	2×1.984(3)	2×1.992(2)	-	2×1.986(2)
Co-O(4) Å	1×1.929(6)	1×1.923(8)	1×1.928(7)	1×1.942(7)	1×1.937(6)
μ_{Co} μ_B	-	2.51(2)	2.08(2)	-	2.32(2)
χ^2	3.04	3.68	3.34	1.71	3.69
R_{nuc}/R_{mag} % [a]	4.8/-	5.3/7.7	4.5/10.8	4.9/-	5.4/12.2

[a] $R_{nuc/mag}=[\sum|(I_{hkl})_{obs}-(I_{hkl})_{calc}|/\sum(I_{hkl})_{obs}]$; (I_{hkl}) is the integrated intensity of the nuclear/magnetic (hkl) reflection.

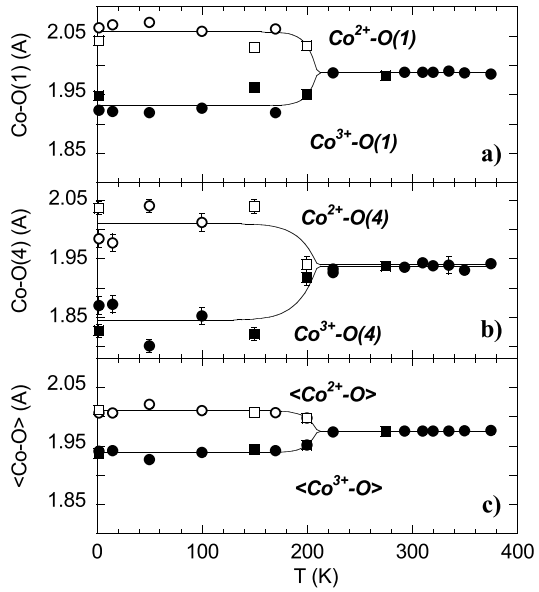

Fig. 2. Temperature dependence of selected Co-O bond lengths and of the mean ⟨Co-O⟩ distance in $HoBaCo_2O_5$. The lines are guide to the eye and the different symbols refer to data collected on different instruments.

3.2 Charge ordered phase

In a first attempt to refine the high resolution NPD patterns in the temperature range $1.5 < T \lesssim T_N$, we applied the Pmmm model with cell parameters $a \sim b \sim a_p$, $c \sim 2a_p$. Here, beside singularities in the isotropic thermal parameters of some cations at the lowest temperatures (mainly non-positive definite values for Co), we also noticed for all compounds an anomaly around 210–220 K in the thermal evolution of the b-axis parameter and of the unit-cell volume (Fig. 1). Since this anomaly was also related to a peak in DSC curves, this suggested the occurrence of a structural phase transition. Further measurements using the cold neutron spectrometer G6-1 revealed the growing of extra peaks below T_{CO} ∼210 K (Fig. 3), which can be indexed using a unit-cell doubled along the b-axis ($a \sim a_p$, $b \sim c \sim 2a_p$). The crystallographic origin of these peaks was confirmed by electron microscopy as will be discussed in the next section. Unobserved Bragg reflections on G6-1 patterns, in particular the (010) at $Q \sim 0.8$ Å^{-1}, implied additional extinction conditions leading to a change of the crystallographic space group from Pmmm to Pmmb.

High resolution NPD patterns below $T_{CO} \sim 210$ K for $HoBaCo_2O_5$ and $T_{CO} \sim 215$ K for $TbBaCo_2O_5$ and $DyBaCo_2O_5$ were thus refined using the Pmmb space group and the doubled unit-cell. The exact values of T_{CO} were determined from G6-1 data as well as DSC and resistivity measurements (see Sect. 4). The results of the refinement in the charge ordered state are summarized in Table 2. The main change in this new structure lies in the existence of two distinct crystallographic sites for the Co cations. Although both sites retain a pyramidal CoO_5 oxygen environment, analysis of the interatomic Co-O distances reveals their sizes differ considerably (Fig. 2). As can be seen in Figure 4, both the O1-basal and the O4-apical oxygen atoms move toward the so called Co1 site. This leads to a smaller volume of the $Co1O_5$ pyramid as evidenced by the evolution of the mean Co-O distances (Fig. 2). With reference to the tabulated ionic radii of Shannon [26], we can reasonably assume the smallest of

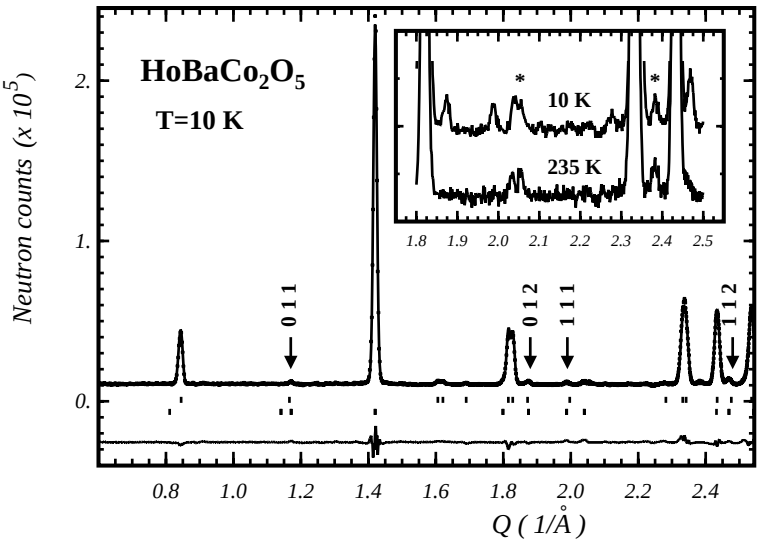

Fig. 3. Observed and calculated NPD spectra of $HoBaCo_2O_5$ collected on G6-1 at 10 K. Top and bottom ticks represent nuclear and magnetic peaks, respectively. Typical CO phase reflections are indicated by arrows, their indexes refer to the unit-cell $a_p \times 2a_p \times 2a_p$. In inset a selected region of NPD patterns collected in the CO and non-CO phases is displayed. The two reflections marked by an asterisk arise from some traces of an impurity phase.

Table 2. Refined structural parameters, selected bond lengths and magnetic moments in the charge ordered state of $LnBaCo_2O_5$. Atomic positions in Pmmb space group are ($\frac{1}{2}$,0,0) for Ln; ($\frac{1}{2}$,0,$\frac{1}{2}$) for Ba; (0,$\frac{1}{4}$,z) for Co(1)/Co^{3+}; (0,$\frac{3}{4}$,z) for Co(2)/Co^{2+}; (0,y, z) for O(1); ($\frac{1}{2}$,$\frac{1}{4}$,z) for O(2); ($\frac{1}{2}$,$\frac{3}{4}$,z) for O(3) and (0,$\frac{1}{4}$,z) for O(4).

	$TbBaCo_2O_5$		$DyBaCo_2O_5$		$HoBaCo_2O_5$	
	100 K	15 K	150 K	15 K	150 K	2 K
a Å	3.8880(2)	3.8861(2)	3.8870(1)	3.8821(1)	3.8804(1)	3.8762(1)
b Å	7.8200(4)	7.8325(3)	7.8363(3)	7.8414(2)	7.8229(2)	7.8265(1)
c Å	7.4797(3)	7.4773(2)	7.4518(1)	7.4430(2)	7.4432(1)	7.4349(1)
$z_{Co(1)/Co^{3+}}$ [a]	0.245(3)	0.249(3)	0.253(4)	0.254(3)	0.251(1)	0.249(2)
$z_{Co(2)/Co^{2+}}$ [a]	0.241(3)	0.241(3)	0.233(4)	0.230(3)	0.231(2)	0.231(2)
$y_{O(1)}$	0.0104(6)	0.013(5)	0.010(2)	0.008(2)	0.0063(6)	0.0077(5)
$z_{O(1)}$	0.1913(8)	0.1916(6)	0.190(1)	0.1897(6)	0.1882(3)	0.1884(3)
$z_{O(2)}$	0.1946(9)	0.1961(2)	0.198(3)	0.185(2)	0.1927(9)	0.1934(9)
$z_{O(3)}$	0.1932(9)	0.1903(2)	0.183(3)	0.196(2)	0.1858(9)	0.1852(9)
$z_{O(4)}$	0.498(1)	0.4983(2)	0.495(4)	0.496(3)	0.495(1)	0.495(1)
Co^{3+}-O(1) Å	2×1.92(2)	2×1.90(2)	2×1.94(2)	2×1.96(2)	2×1.96(1)	2×1.95(1)
Co^{3+}-O(2) Å	2×1.98(1)	2×1.98(2)	2×1.986(8)	2×2.009(6)	2×1.988(6)	2×1.981(5)
Co^{3+}-O(4) Å	1×1.89(8)	1×1.86(8)	1×1.80(4)	1×1.80(3)	1×1.82(3)	1×1.83(3)
Co^{2+}-O(1) Å	2×2.07(2)	2×2.09(2)	2×2.07(1)	2×2.05(2)	2×2.03(1)	2×2.04(1)
Co^{2+}-O(3) Å	2×1.98(1)	2×1.98(2)	2×1.979(7)	2×1.958(3)	2×1.969(5)	2×1.968(4)
Co^{2+}-O(4) Å	1×1.95(8)	1×1.95(8)	1×2.03(4)	1×2.03(3)	1×2.04(3)	1×2.04(3)
$\mu_{Co(1)}$ μ_B [b]	3.3(1)	3.4(2)	3.8(1)	3.8(1)	3.73(8)	3.79(9)
$\mu_{Co(2)}$ μ_B [b]	2.6(1)	2.9(2)	2.8(1)	2.9(1)	2.76(9)	2.93(9)
χ^2	4.28	5.31	2.04	2.11	4.66	5.20
R_{nuc}/R_{mag} %	12.7/14.2	12.6/8.9	3.8/7.1	4.08/9.68	6.3/6.7	7.0/10.5

[a]Based on Bond Valence Calculations, we have attributed the Co(1) and Co(2) sites to the Co^{3+} and Co^{2+} species, respectively.
[b]Rietveld refinement using exchanged values for the magnetic moments of Co(1) and Co(2) yields similar R factors. The present attribution of magnetic moments refers to the model involving HS-Co^{3+} (see text).

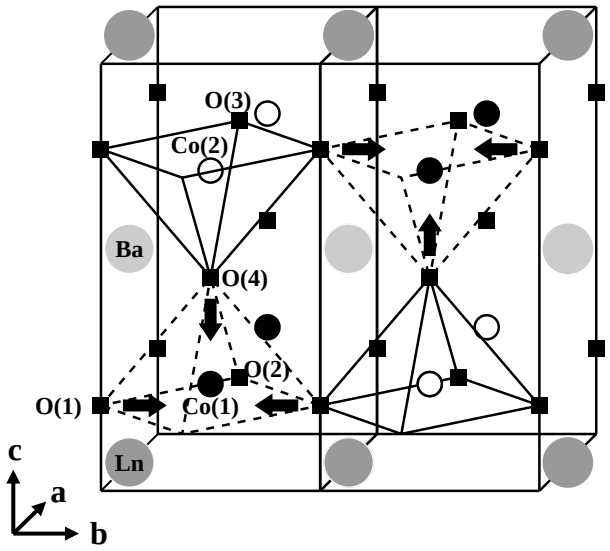

Fig. 4. Crystallographic unit-cell of $LnBaCo_2O_5$ in the CO state. Arrows indicate the major modifications of the CoO_5 pyramids compare to the high temperature phase.

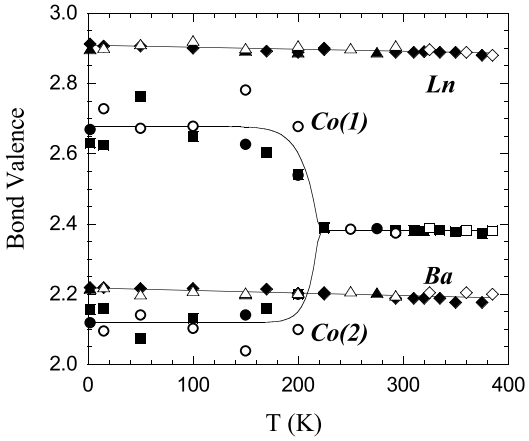

Fig. 5. Temperature dependence of the calculated cation Bond Valences in $HoBaCo_2O_5$ (black symbols) and $TbBaCo_2O_5$ (white symbols). The lines are guide to the eye.

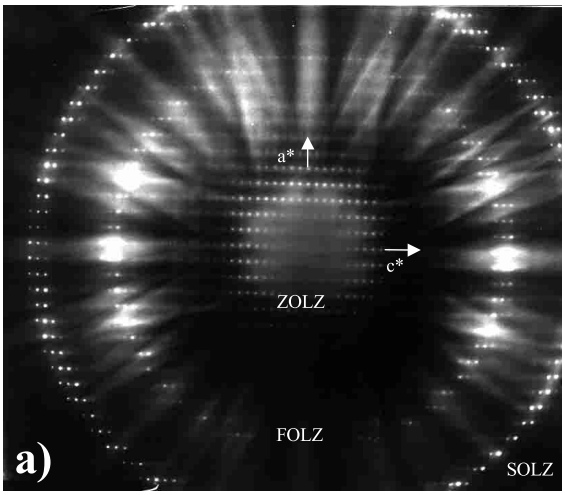

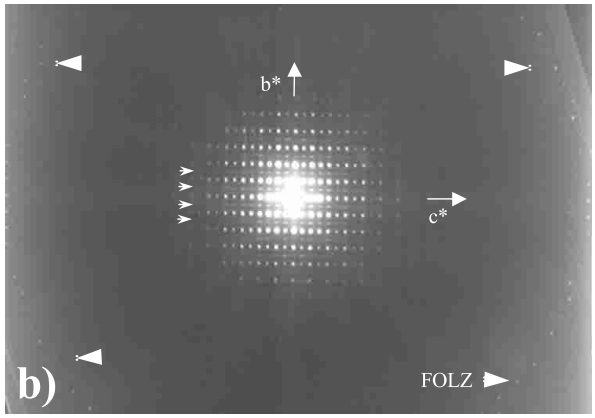

Fig. 6. (a) [010]-microdiffraction low temperature pattern of $HoBaCo_2O_5$ showing Zero, First and Second Order Laue Zones. From FOLZ diameter, the direct b parameter is calculated to be $\sim 2a_p$. (b) [100]-microdiffraction low temperature pattern of $TbBaCo_2O_5$ showing the extra-dots (small white arrows) owing to the doubling of the direct b parameter. Measurement of FOLZ diameter confirm the direct a parameter is equal to a_p.

the pyramids, that is the Co1 site, occupied by the Co^{3+} ions exclusively. This picture is further confirmed by bond valence calculations yielding approximate valences of +2.7 for the Co1 site and +2.1 for the Co2 site as soon as T is below T_{CO} (Fig. 5). Hence, each of the Co1 and Co2 site can be considered to be exclusively occupied by the Co^{3+} and Co^{2+} species occurring in $LnBaCo_2O_5$ (Ln = Tb, Dy, Ho). This feature is further confirmed by the almost $1\mu_B$ difference of the refined saturated magnetic moment of these two sites. The resulting charge ordered structure can thus be described by an alternate stacking of $Co^{2+}O_5$ and $Co^{3+}O_5$ pyramids along the b- and c-directions, and $Co^{2+}O_5$ or $Co^{3+}O_5$ pyramids files along the a-direction.

Electron diffraction (ED) study confirmed for $LnBaCo_2O_5$ (Ln = Ho, Tb) the doubling along b of the crystallographic cell at low temperature. Indeed, extra spots, vanishing at room temperature, were clearly visible at low temperature (93 K) on [100] Selected Area Electron Diffraction (SAED) pattern. However, mainly due to multiple scattering effects, it is not always possible from SAED only to unambiguously assess on the extinction conditions. In this case, combination of SAED with electron microdiffraction allows the confirmation of the low temperature Pmmb space group which is characterized by the only reflection existence conditions: $hk0, k = 2n$. Furthermore, the electron microdiffraction method yields simultaneous observations of both Zero Order Laue Zone (ZOLZ) and First Order Laue Zone (FOLZ), and thus measurement of the reciprocal perpendicular axis. As can be seen in Figure 6a, [010]-microdiffraction pattern on $HoBaCo_2O_5$ shows $h0l$ (ZOLZ) and $h1l$ (FOLZ) reflections with no existence conditions on $h0l$-type reflections. From the measurement of the diameter of FOLZ, we evaluate the direct b parameter as close to $2a_p$. On the other hand, the FOLZ diameter of [100]-microdiffraction pattern

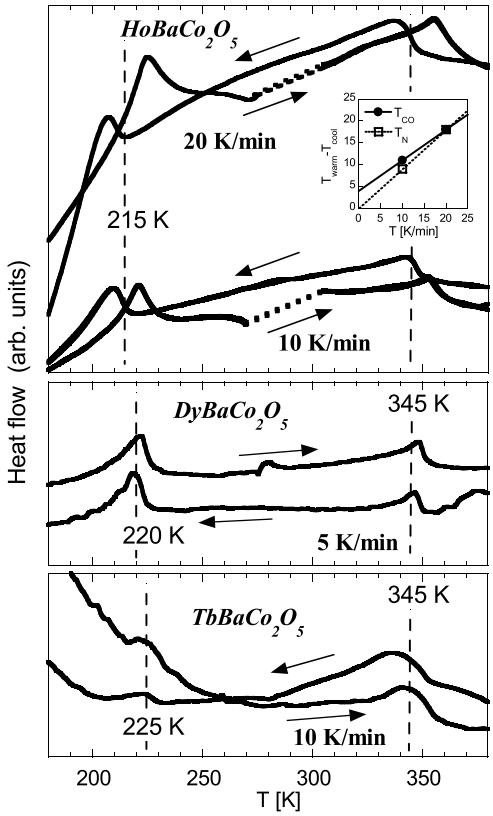

Fig. 7. Temperature dependence of DSC data measured on heating and cooling runs in (a) $HoBaCo_2O_5$ at two distinct heating/cooling rates and in (b) $DyBaCo_2O_5$ and (c) $TbBaCo_2O_5$. The ordinate indicates endothermic (exothermic) reaction for heating (cooling) runs. In inset, we have plotted the difference of T_N and T_{CO} of $HoBaCo_2O_5$ as determined from cooling and heating runs *vs.* the temperature variation rate. Values extrapolated to zero are representative of the order character of the transition.

measured on $TbBaCo_2O_5$, leads to $a \sim a_p$, confirming thus the crystallographic cell is not doubled along this direction (Fig. 6b). On the same pattern, a closer examination of the ZOLZ allows to distinguish additional spots, with no existence conditions on $0kl$-type reflections, which is indicative of the the doubling along the b-direction.

4 Transport properties

Figure 7 shows Differential Scanning Calorimetry (DSC) measurements performed on $LnBaCo_2O_5$ (Ln = Tb, Dy, Ho). The DSC curves exhibits two exothermic (endothermic) peaks around T_N and T_{CO} in cooling (heating) runs. These peaks are consistent with entropy change caused by spin and charge ordering at T_N and T_{CO}, respectively. The observed shifts of the peak maximum between cooling and heating runs, ΔT_N and ΔT_{CO}, suggest an hysteretic behavior for these transitions. In order to carefully check the order of the transitions, DSC data were collected on $HoBaCo_2O_5$ at two distinct heating/cooling

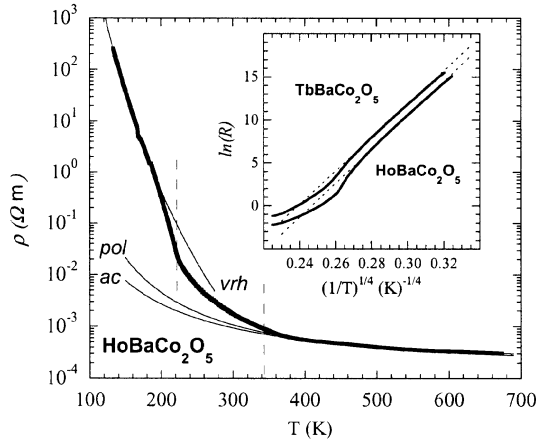

Fig. 8. Temperature dependence of the resistivity measured in $HoBaCo_2O_5$. In inset, $\ln(\rho)$ *vs.* $1/T$ curve of resistivity in $LnBaCo_2O_5$ (Ln = Ho, Tb). Solid lines (dash lines in the inset) are fit to the data using models described in text.

rates (10 K/min and 20 K/min). From the values extrapolated to zero temperature variation rate, $\Delta T_N \sim 0$ K and $\Delta T_{CO} \sim 4$ K , we assume the transitions at T_N and T_{CO} are of second and first order character, respectively (see inset in Fig. 7). Finally, we notice an increase of T_{CO} when increasing the size of the rare earth ion, whereas T_N remains almost constant.

As shown in Figure 8, both $HoBaCo_2O_5$ and $TbBaCo_2O_5$ compounds exhibit insulating behavior over the whole measured temperature range (90–700 K for Ho, 90–380 K for Tb). Furthermore, resistivity data collected under an external magnetic field of 5 tesla clearly indicate the absence of relevant magnetoresistive effects in our compounds. The onset of spin and charge ordering transitions appears in the resistivity curves as two discontinuities tending to reinforce the insulating character. In order to better determine T_{CO} in $LnBaCo_2O_5$ (Ln = Ho, Tb) from resistivity measurements, we have plotted the thermal dependence of the activation energy $E_{ac} = \mathrm{d}\ln(\rho)/\mathrm{d}(1/T)$, when assuming a simple activation model. As shown in Figure 9, we clearly observe a first increase of the activation energy at the onset of spin ordering followed by steep rise at the charge ordering temperature. The weak hysteretic behavior of the transition at T_{CO} is confirmed by the slight difference of the peak maximum between cooling and heating runs. Two regimes can be distinguished for the temperature dependence of the resistivity, which can be approximated by usual model for insulating oxides [27]. Below T_{CO}, the resistivity is best approximated using a Variable Range Hopping model (VRH), $\rho_{vrh} = \rho_o \exp((T_o/T)^{1/4})$, with $T_o = 1.4 - 1.5 \times 10^9$ K (see inset of Fig. 8). In VRH theory, $k_B T_o \approx 21/[\zeta^3 N(E_F)]$ where ζ is the decay length of the localized wave function and $N(E_F)$ the density of localized states at the Fermi level. Assuming $\zeta \approx a_p \approx 3.9$ Å, we find $N(E_F) \sim 2.8 \times 10^{18}$ eV^{-1} cm^{-3}, a typical value for disorder semiconductors. Above T_N, either a simple activation model, $\rho_{ac} = \rho_o \exp(E_{ac}/kT)$, or a small polaron model, $\rho_{pol} = \rho_o T \exp(E_{pol}/kT)$, reproduces equally well

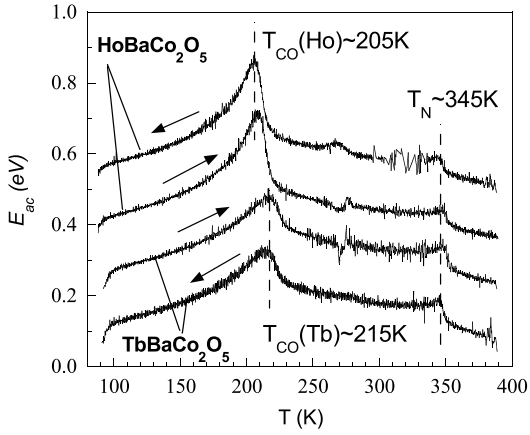

Fig. 9. Temperature dependence of the activation energy $E_{\rm ac}$ in $LnBaCo_2O_5$ (Ln = Ho,Tb). An offset of 0.15 eV is successively applied to the curves.

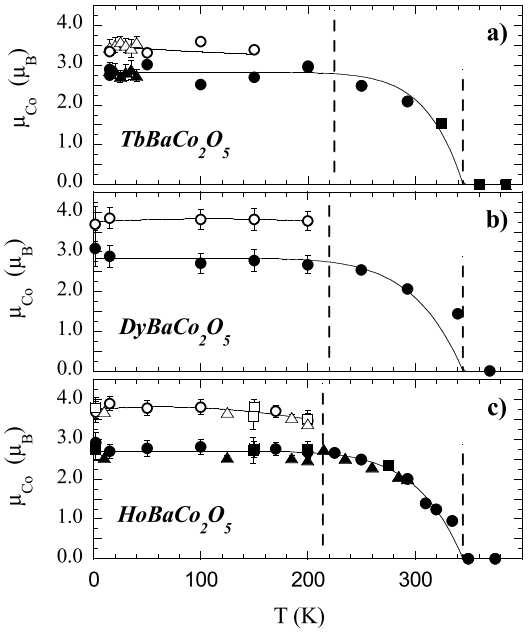

Fig. 10. Temperature dependence of Co magnetic moments in (a) $TbBaCo_2O_5$, (b) $DyBaCo_2O_5$ and (c) $HoBaCo_2O_5$. The lines are guide to the eye and the different symbols refer to data collected on different instruments.

the data. In $HoBaCo_2O_5$, for which resistivity was measured at sufficiently high temperatures, the refined activation energies are $E_{\rm ac} = 0.055$ eV or $E_{\rm pol} = 0.096$ eV. In the intermediate temperature region, $T_{\rm CO} < T < T_{\rm N}$, none of the above models is able to reproduce the measured resistivity. This range might thus be interpreted as a transition regime from a preliminary partial charge localization at $T_{\rm N}$ to the well charge localized state below $T_{\rm CO}$. Usually, the coincident increase of resistivity and the onset of an AF state would lead us to conclude, similarly to observations made in manganites [28,29] or nickelates [30], to a preliminary charge ordering at $T_{\rm N}$. However, no indication of long-range CO effects was detected in our diffraction data. It is likely that below $T_{\rm N}$ a preliminary partial charge localization occurs, the origin of which is not clearly established but is surely related to the Co spin ordering. In the AF-charge disordered state, there is a competition between the Co^{2+}-Co^{2+}, Co^{3+}-Co^{3+} and Co^{2+}-Co^{3+} couplings along all three crystallographic axes. In the latter coupling, depending on the spin state of Co^{3+} (see Sect. 5), either a $d_{x^2-y^2}$- or a d_{xz}-type electron is not completely localized on one of the cobalt ions. Hence, electron hoping over Co^{2+}-Co^{3+} distances range remain possible in all crystallographic directions. Below $T_{\rm CO}$, the $d_{x^2-y^2}$ or d_{xz} electrons are well localized on the Co^{2+} site, leading to the CO phase, and $LnBaCo_2O_5$ becomes highly insulating.

5 Magnetic and electronic structure

We have characterized the magnetic behavior of all three samples using neutron diffraction. For $LnBaCo_2O_5$ (Ln = Tb, Dy, Ho) compounds, magnetic peaks appear below $T_{\rm N} \sim 340$ K, corresponding to the occurrence of the long-range antiferromagnetic order of Co atoms. These peaks are indexed with the propagation vector ($\frac{1}{2}$ $\frac{1}{2}$ 0) in the '$a_{\rm p} \times a_{\rm p} \times 2a_{\rm p}$' unit-cell. This so called G-type magnetic structure is characterized by the Co atoms antiferromagnetically coupled with their six nearest Co neighbors along the three crystallographic axes. Magnetic moments lie in the *ab*-plane. Since the *a* and *b* cell parameters are too close in the charge disordered phase, it is impossible to determine precisely the direction of the moments from refinement of NPD data only. Nevertheless, in agreement with the realized orientation in the CO state, we assume the magnetic moments pointing along the *a*-direction in the temperature range 210 K $< T <$ 340 K. This picture was furthermore favored by electric field gradient calculations issued from room temperature Mössbauer spectroscopy data we have recently performed on a 1% ^{57}Fe-doped $HoBaCo_2O_5$ compound [31]. In the charge ordered phase, $T < T_{\rm CO}$, the magnetic unit-cell remains unchanged. However, since the crystallographic cell is now doubled ('$a_{\rm p} \times 2a_{\rm p} \times 2a_{\rm p}$'), the antiferromagnetic structure is described using a propagation vector ($\frac{1}{2}$ 0 0). Here again because of the extinction of the particular ($\frac{1}{2}$ 0 0) reflection at $Q \sim 0.8$ Å^{-1} (see Fig. 3), the Co magnetic moments are necessarily pointing along the *a*-axis. In the CO state with Pmmb crystallographic space group, there are two Co sites, resulting in two independent magnetic moments. From refinement of NPD data, the calculated values of Co moments at saturation are $\sim 3.7\mu_{\rm B}$ and $\sim 2.7\mu_{\rm B}$ for $LnBaCo_2O_5$ (Ln = Tb, Dy, Ho) (Fig. 10). The almost $1\mu_{\rm B}$ difference, meaning a one electron difference, confirm the Co^{2+} and Co^{3+} charge ordered picture previously deduced from crystallographic considerations only. Furthermore the $1\mu_{\rm B}$ difference sets in almost instantaneously at ($T < T_{\rm CO}$) and is retained down to the lowest measured temperature. At this point, we have to note that an interchange in the assignment of Co1/Co2 site moment values result in equally good refinement. Therefore

the precise assignment of the maximal magnetic moment to either Co1 or Co2 is not possible from refinement of NPD data only. As a consequence, we have to discriminate between the two following equally probable models.

In the first one, which was used in our previous interpretation of NPD results on $HoBaCo_2O_5$ [10], we attribute the $\sim 3.7\mu_B$ and $\sim 2.7\mu_B$ magnetic moment values to Co^{3+} and Co^{2+} ions, respectively. Assuming a totally quenched orbital contribution, these values are in good agreement with spin-only values of high spin state cobalt HS-Co^{3+} and HS-Co^{2+} ions. Indeed, for HS-Co^{3+} ($t_{2g}^4 e_g^2, S = 2$) and HS-Co^{2+} ($t_{2g}^5 e_g^2, S = 3/2$), the maximum spin-only values we can expect from refinement of NPD data are $4\mu_B$ and $3\mu_B$, respectively [32]. In this case, the slight reduction from the ideal moment values might be attributed to covalency effects and/or zero point motion since the magnetic structure is antiferromagnetic [33]. This picture is in total agreement with the Goodenough-Kanamori (GK) rules of superexchange magnetism, which predict strong antiferromagnetic interactions in all three crystallographic directions [21,22]. Indeed, for all the possible HS-Co^{3+}-HS-Co^{3+}, HS-Co^{2+}-HS-Co^{2+} and HS-Co^{3+}-HS-Co^{2+} bondings, the magnetic interaction is dominated by $(e_g - p_\sigma - e_g)$-type AF couplings: $d_{3z^2-r^2} - p_z - d_{3z^2-r^2}$ along c, $d_{x^2-y^2} - p_{x(y)} - d_{x^2-y^2}$ and $d_{xy} - p_{x(y)} - d_{xy}$ along $a(b)$ (Fig. 11). This match ideally to the relatively high T_N antiferromagnetic structure observed in $LnBaCo_2O_5$ (Ln = Y, Ho, Tb). For this reason mainly, we have chosen this solution in our previous description of $HoBaCo_2O_5$ [10], which moreover appears now further supported by (LSDA)+U band-structure calculations [19].

The second picture, introduced by Vogt *et al.* for $YBaCo_2O_5$ [9], implies the occurrence of Co^{3+} ions in the intermediate spin (IS) state ($t_{2g}^5 e_g^1, S = 1$). Note that this model is also supported by another work using one-electron band-structure calculations in the local-spin-density-approximation (LSDA)+U method [20]. Here, the $\sim 3.7\mu_B$ and $\sim 2.7\mu_B$ magnetic moment values are attributed to HS-Co^{2+} and IS-Co^{3+} ions, respectively. Since the highest expected spin-only values measurable by NPD are $2\mu_B$ (resp. $3\mu_B$) for a S=1 (resp. S=3/2) spin system, only a non negligible orbital contribution to the magnetic moment is able to account for the higher magnetic moments measured in $LnBaCo_2O_5$ (Ln = Y, Tb, Dy, Ho). In their calculations, Kwon *et al.* [20] estimates an orbital contribution of $1\mu_B$ and $0.4\mu_B$ for HS-Co^{2+} and IS-Co^{3+}. Note that orbital contribution is more likely to occur in the end transition metal series in general, and in the Co case in particular. This second picture, however, requires a more subtle interpretation of the qualitative GK rules in order to describe the G-type antiferromagnetic structure measured in $LnBaCo_2O_5$ (Ln = Y, Tb, Dy, Ho). In the Figure 11, we have represented the orbital d levels for Co ions in pyramidal crystal field environment [15]. The major difference between HS-Co^{3+} and IS-Co^{3+} resides in the occupation of the $d_{x^2-y^2}$ orbital of highest energy. This leads to a possible change of the sign of the superexchange coupling in the ab-plane (Fig. 11). Indeed, contrary

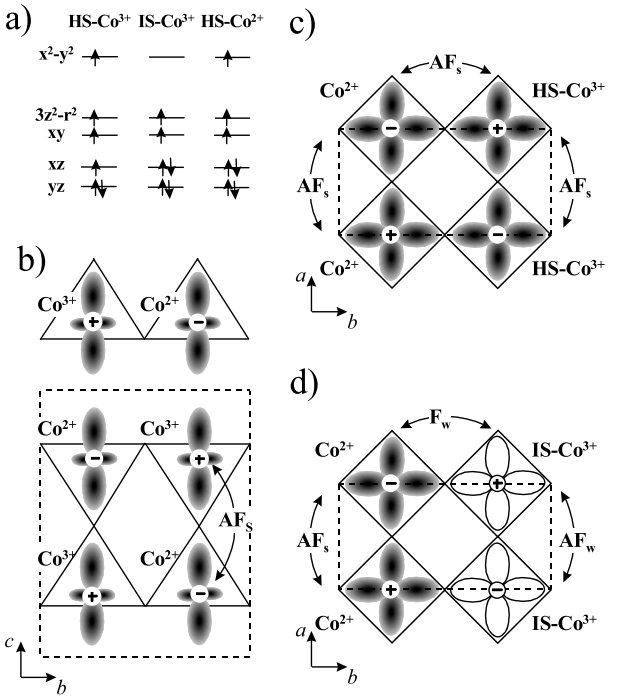

Fig. 11. (a) Crystal field splitting diagram for slightly distorted square base pyramidal environment and electronic configuration of the different Co ions assumed to occur in $LnBaCo_2O_5$. (b) Superexchange coupling along c valid for both models involving either IS-Co^{3+} or HS-Co^{3+} ions. 180°-type superexchange coupling in the ab-plane as predicted from Goodenough-Kanamori rules when (c) HS-Co^{3+} ions or (d) IS-Co^{3+} ions are involved. Grey/white color denotes half occupied/empty orbitals. AF_s, AF_w and F_w means strong, weak antiferromagnetic coupling and weak ferromagnetic coupling.

to the measured magnetic structure, a weak ferromagnetic IS-Co^{3+}-HS-Co^{2+} coupling is predicted along the b-direction according to the GK rules, at least in the ideal case of 180° bonding and as long as $d_{x^2-y^2} - p_\sigma - d_{x^2-y^2}$ is considered as the dominant interaction. Having said that, two explanations can be advanced to recover the effective AF interaction along b measured by NPD. In $LnBaCo_2O_5$ (Ln = Y, Ho, Tb, Dy), the Co-O-Co angles are ~155° in the ab-plane and thus a change of the superexchange sign is highly probable. Secondly, there is a competition between the $d_{x^2-y^2} - p_\sigma - d_{x^2-y^2}$ interaction and the $d_{xy} - p_\pi - d_{xy}$ coupling, which is clearly antiferromagnetic. In conclusion, we point out that the Co-Co magnetic coupling in the ab-plane appears qualitatively weaker for intermediate spin states than for high spin states. Only, the Co^{3+}-Co^{2+} exchange along c remains globally unchanged between the two spin state picture.

In the AF charge disordered state, $T_{CO} < T < T_N$, the magnetic moments on the unique Co site is not saturated as can be seen in Figure 10. Furthermore, we do not observe any discontinuity in the thermal dependence of the magnetic moment down to T_{CO}. Near room temperature, the calculated moments, $2\mu_B$ per cobalt ion for all three

measured compounds $LnBaCo_2O_5$ (Ln = Tb, Dy, Ho), are very similar to the value reported in $YBaCo_2O_5$ [9]. In order to explain this "reduced" moment, Vogt *et al.* argued the Co^{2+} ions are necessarily in low-spin (LS) state ($t_{2g}^6 e_g^1, S = 1/2$) which, together with IS-Co^{3+}, would thus lead to an expected spin-only value of $1.5\mu_B$ for the magnetic moment on the Co site (and not the $1.73\mu_B$ value given in Ref. [9]) [32]. Based on this argument only, Vogt *et al.* claimed the occurrence of a low to high spin state transition in $YBaCo_2O_5$. Although our results are similar to the $YBaCo_2O_5$ parent case, we do not go as far as to say there is a spin state transition in $LnBaCo_2O_5$ (Ln = Tb, Dy, Ho). As seen above, assessment on the realized electronic structure of the Co ions is not obvious based on refined magnetic moment values only. This is furthermore valid when the moments have not reached their saturated values, which is clearly the case in the AF charge disordered state of $LnBaCo_2O_5$ (Ln = Tb, Dy, Ho). Additional information on the actual electronic structure above T_{CO} could be experimentally gained from magnetic susceptibility measurements. Indeed, the effective magnetic moments μ_{eff} can be extracted by fitting to a Curie-Weiss law the high temperature magnetic susceptibility data. Hence, the resulting value can be compared with the several potential electronic pictures expected for paramagnetic Co ions in a mixed valence state. A nice example illustrating this type of experiment was given by Moritomo *et al.* in their study of $TbBaCo_2O_{5.5}$ [12]. There, a spin state transition of the Co^{3+} ion was qualitatively evidenced by an abrupt fall of μ_{eff} at the metal-insulator transition T_{MI} ∼340 K, but still in the paramagnetic state. Note that in that case, the refined values, $\mu_{eff} \sim 4.4\mu_B$ and $\sim 7.1\mu_B$, are much higher than theoretical values for IS-Co^{3+} and HS-Co^{3+}, even if considering spin-orbit coupling. This is finally not surprising since the paramagnetic Tb ions also contribute to the effective magnetic moment. In $LnBaCo_2O_5$ (Ln = Ho,Tb), the strong paramagnetic signal induced by the rare earth ion partially masks the signal arising from the Co ions. It therefore prevents any quantitative analysis of the effective moment refined from susceptibility data making vain any attempt to unambiguously determine the spin-state of the Co ions using this technique. Finally, whereas both band structure calculations performed on the basis of the structural data of $YBaCo_2O_5$ differ on the realized electronic state of the Co^{3+} ions at the lowest temperatures [19,20], any of both studies conclude to the occurrence of a spin state transition at T_{CO}.

So far we have not mention the magnetic behavior of the rare earth ions in $LnBaCo_2O_5$ (Ln = Tb, Dy, Ho). As shown in Figure 12, we clearly observed on NPD patterns additional reflections growing below ∼ 4 K in $TbBaCo_2O_5$. These additional magnetic peaks are indexed with a $(\frac{1}{2}\ 0\ \frac{1}{2})$ propagation vector and result in an antiferromagnetic ordering of the Tb^{3+} ions along all the three crystallographic axes. The Tb^{3+} magnetic moments point along the *c*-direction and amount to $\sim 5.6\mu_B$ at the lowest measured temperature (1.5 K), that is far below the expected free ion value ($9\mu_B$). Although the reduction from the free ion value can be accounted for by crystalline electric field effects, we however suspect the Tb magnetic moments have not reached saturation at 1.5 K in $TbBaCo_2O_5$. As can be seen in the Figure 12, the width of the Tb induced magnetic peaks are considerably broader than nuclear Bragg reflection or Co induced equivalent (this effect appears even much better in high resolution NPD patterns). Therefore, we think the long-range ordering of the Tb magnetic moments is still not completely established at 1.5 K. In the $HoBaCo_2O_5$ and $DyBaCo_2O_5$ cases, there is no indication of rare earth moment ordering down to 1.5 K. However, it is likely that similarly to the Tb equivalent compound, long-range magnetic ordering of Ho/Dy ions occurs at lower temperatures.

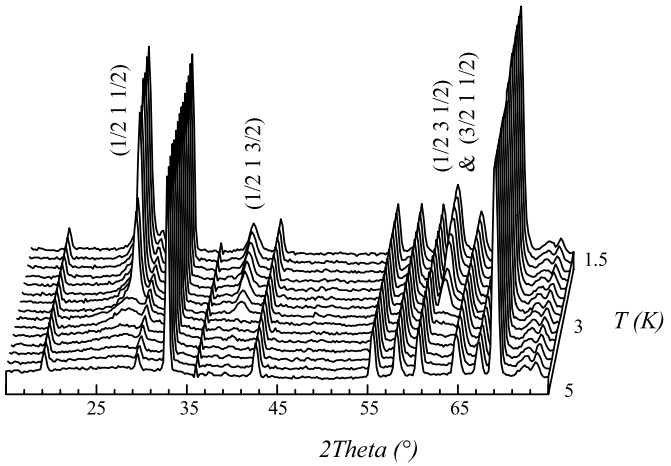

Fig. 12. NPD patterns of $TbBaCo_2O_5$ collected on D1B in the temperature range 1.5–5 K. Additional peaks growing below $T_N(Tb) \sim 4$ K correspond to the onset of AF Tb ordering.

6 Conclusion

In this paper, we have clearly demonstrated the strong interplay of the crystallographic, magnetic and transport properties in $LnBaCo_2O_5$ (Ln = Tb, Dy, Ho). The crystallographic transition due to the charge ordering state was directly evidenced using both neutron and electron diffraction techniques. The CO picture was further supported by indirect methods such as careful examination of the bond distances, the bond valences as well as the refined magnetic moments extracted from high resolution NPD data. Transport measurements appeared to give valuable information on the transition temperatures. From neutron powder diffraction experiments only we can not unambiguously assess on the realized electronic structure of the transition metal ions. In particular, we can not discriminate between the two probable models involving Co^{3+} ions either in high spin state or in intermediate spin state. The observed G-type AF magnetic structure does not provide additional information since both models may be qualitatively explained by the Goodenough-Kanamori rules for superexchange. We expected to obtain a preliminary indication on the correct model from theoretical calculations.

Such studies, using (LSDA)+U method, have been performed for $LaCoO_3$ [34] and $YBaCo_2O_5$ [19,20], two systems for which doubts remain about the actual electronic configuration of Co^{3+} ions. In $LaCoO_3$ and in $YBaCo_2O_5$, according to reference [20], the IS-Co^{3+} state appeared energetically more favorable. Therefore, owing to the similitude of the magnetic and crystallographic structure exhibited by $YBaCo_2O_5$ and $LnBaCo_2O_5$ (Ln = Tb, Dy, Ho), a picture with IS-Co^{3+} and HS-Co^{2+} can be considered as well in our measured compounds. On the other hand, similar calculations performed by another group [19] conclude that the Co^{3+} ions are in high-spin state over the whole temperature range and therefore confirm our model. As can be seen from these contradictory results, the question of the Co^{3+} spin state remains open. Nevertheless, a more definitive answer could be experimentally obtained using the recently developed X-ray (resonant or non-resonant) magnetic scattering techniques [35] or the resonant X-ray dichroism [36]. Both methods allow the separate observation of spin- and orbital-moment densities, which could thus confirm or amend the hypothesis of negligible orbital contribution. Mössbauer spectroscopy could be a useful tool as well owing to its ability to provide information on the oxidation- and spin-state of transition metals. Our preliminary Mössbauer measurements performed on slightly ^{57}Fe doped compounds were not really conclusive in this sense. In fact, doubts will still remain whether the ^{57}Fe and the Co ions exhibit the same behavior in $LnBaCo_2O_5$. A better operating way would be to use ^{57}Co isotope as absorber/emitter. Finally, we can mention the inelastic neutron scattering on single crystal, which from the study of collective magnetic excitations, allows the quantitative determination of the individual magnetic coupling parameters J(Co-Co) along all three crystallographic directions.

At this stage, we have to mention two points which will deserve particular attention in the forthcoming studies of the $LnBaCo_2O_5$ compounds. Although the Co-Co interactions through the oxygen atoms are well explained within the superexchange framework, there is still an ambiguity about the Co^{2+}-Co^{3+} coupling through the oxygen vacant Ln-layer. Direct exchange only, expected to be ferromagnetic, appears improbable from the small orbital overlap. Therefore superexchange-type mechanisms involving different paths may be postulated. In particular, we cannot completely rule out the participation of the rare-earth ion orbitals to the superexchange magnetism. In any case, a better knowledge of the coupling over the Ln-layer can be gained from a complete study of the $LnBaCo_2O_{5+\delta}$ ($0 \leq \delta \leq 1$) systems, for which there are oxygen ions available for cobalt superexchange coupling. The second point concerns the occurrence of the well established long-range charge ordering far below the onset of magnetic ordering, which is unique in the perovskite-based compound series. As evidenced by resistivity measurements, a partial and preliminary charge localization seems to set in in the intermediate temperature range $T_{CO} < T < T_N$. A closer study of the relaxation of the magnetic moments in the $T_{CO} < T < T_N$ temperature range (typically using μSR techniques) could eventually allow to distinguish between either no charge ordering or dynamical and/or statistical short-range charge order. This is a key issue in understanding the strongly correlated electron properties of these materials.

The authors thank Dr. G. Baldinozzi for performing some of the DSC measurements and Dr. U. Staub for scientific discussions.

References

1. R. Mahendiran, A.K. Raychaudhuri, A. Chainani, D.D. Sarma, J. Phys. C **10**, L562 (1995).
2. C. Martin, A. Maignan, D. Pelloquin, N. Nguyen, B. Raveau, Appl. Phys. Lett. **71**, 1421 (1997).
3. Y. Moritomo, M. Takeo, X.J. Liu, T. Akimoto, A. Nakamura, Phys. Rev. B **58**, R13334 (1998).
4. I.O. Troyanchuk, N.V. Kasper, D.D. Khalyavin, A.N. Chobot, G.M. Chobot, H. Szymczak, J. Phys. C **10**, 6381 (1998).
5. A. Maignan, C. Martin, D. Pelloquin, N. Nguyen, B. Raveau, J. Solid State Chem. **142**, 247 (1999).
6. D. Akahoshi, Y. Ueda, J. Phys. Soc. Jpn **68**, 736 (1999).
7. I.O. Troyanchuk, N.V. Kasper, D.D. Khalyavin, A.N. Chobot, G.M. Chobot, H. Szymczak, J. Phys. C **12**, 2485 (2000).
8. W. Zhou, C. Tian Lin, W. Yao Liang, Adv. Mater. **5**, 735 (1993).
9. T. Vogt, P.M. Woodward, P. Karen, B.A. Hunter, P. Henning, A.R. Moodenbaugh, Phys. Rev. Lett. **84**, 2969 (2000).
10. E. Suard, F. Fauth, V. Caignaert, I. Mirebeau, G. Baldinozzi, Phys. Rev. B **61**, R11871 (2000).
11. E. Suard, F. Fauth, V. Caignaert, Physica B **276–278**, 254 (2000).
12. Y. Moritomo, T. Akimoto, M. Takeo, A. Machida, E. Nishibori, M. Takata, M. Sakata, K. Ohoyama, A. Nakamura, Phys. Rev. B **61**, R13325 (2000).
13. W. Zhou, Chem. Mater. **6**, 441 (1996).
14. D. Akahoshi, Y. Ueda, J. Solid State Chem. **156**, 355 (2001).
15. J.J. Zuckermann, J. Chem. Educ. **42**, 135 (1965).
16. K. Yamura, Q. Huang, R.W. Erwin, J.W. Lynn, R.J. Cava, Phys. Rev. B **60**, 9623 (1999).
17. J. Hernàndez-Velasco, R. Sàez-Puche, A. Hoser, J. Rodriguez-Carvajal, Physica B **276-278**, 726 (2000), and references therein.
18. J.H. Fjellvåg, B. Hauback, R. Bredesen, J. Mater. Chem. **7**, 2415 (1997).
19. Hua Wu, Phys. Rev. B **62**, R11953 (2000).
20. S.K. Kwon, J.H. Park, B.I. Min, Phys. Rev. B **62**, R14637 (2000).
21. J.B. Goodenough, Phys. Rev. **100**, 564 (1955).
22. J. Kanamori, J. Phys. Chem. Solids **10**, 87 (1959).
23. F. Millange, V. Caignaert, B. Domengès, B. Raveau, Chem. Mater. **10**, 1974 (1998).
24. J. Rodriguez-Carvajal, Physica B **192**, 55 (1993).

25. A.S. Wills, I.D. Brown, VaList, CEA, France, 1999.
26. R.D. Shannon, Acta Cryst. A **32**, 751 (1976).
27. G.J. Snyder, C.H. Booth, F. Bridges, R. Hiskes, S. DiCarolis, M.R. Beasley, T.H. Geballe, Phys. Rev. B **55**, 6453 (1997).
28. N. Kumar, C.N.R. Rao, J. Solid State Chem. **129**, 363 (1997).
29. P.G. Radaelli, D.E. Cox, M. Marezio, S.-W. Cheong, Phys. Rev. B **55**, 3015 (1997).
30. J.A. Alonso, J.L. Garcia-Munoz, M.T. Fernández-Díaz, M.A.G. Aranda, M.J. Martínez-Lope, M.T. Casais, Phys. Rev. Lett. **82**, 3871 (1999).
31. V. Caignaert (private communication).
32. In their study on $YBaCo_2O_5$, Vogt *et al.* [9] make a somewhat frequent mistake in comparing the magnetic moments refined from neutron diffraction data with the effective free ion moment value which is $\mu_{\rm SO} = 2\sqrt{S(S+1)}$ for a spin state S. This is not correct since the spin-only neutron scattering value for a localized model corresponds to the sum of the unpaired electron. The correct value is thus $\mu_{SO} = 2S$ for a spin state S.
33. B.C. Tofield, *The Study of Covalency by Magnetic Neutron Scattering*, Vol. 21 of *Structure and Bonding* (Springer Verlag, Berlin, 1975).
34. M.A. Korotin, S.Yu. Ezhov, I. Solovyev, V.I. Anisimov, D.I. Khomskii, G.A. Sawatzky, Phys. Rev. B **54**, 5309 (1996).
35. V. Fernandez, C. Vettier, F. de Bergevin, C. Giles, W. Neubeck, Phys. Rev. B **57**, 7870 (1998).
36. J. Stöhr, H. König, Phys. Rev. Lett. **75**, 3748 (1995).